AD-A178 550

AFWAL TR-86-4103
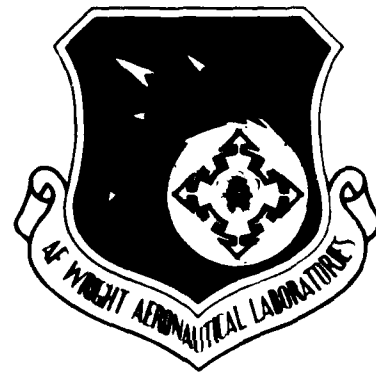
MODELING OF SUBSTRATE AND IMPLANTATION EFFECTS ON THE THRESHOLD
VOLTAGE OF MESFET STRUCTURES FABRICATED IN SEMI-INSULATING GaAs

Thomas W. Sigmon

Stanford Electronics Laboratory
Stanford University
Stanford, CA 94305

December 1986

Final Report for Period September 1984 - May 1986

REPORT DOCUMENTATION PAGE *AI78550*

Form Approved
OMB No. 0704-0188

1a REPORT SECURITY CLASSIFICATION	1b RESTRICTIVE MARKINGS
Unclassified	

2a. SECURITY CLASSIFICATION AUTHORITY	3 DISTRIBUTION/AVAILABILITY OF REPORT
	Distribution for public release; distribution is unlimited
2b. DECLASSIFICATION/DOWNGRADING SCHEDULE	

4 PERFORMING ORGANIZATION REPORT NUMBER(S)	5 MONITORING ORGANIZATION REPORT NUMBER(S)
	AFWAL-TR-86-4103

6a NAME OF PERFORMING ORGANIZATION	6b OFFICE SYMBOL (If applicable)	7a NAME OF MONITORING ORGANIZATION
Stanford Electronics Laboratory Stanford University		Air Force Wright Aeronautical Laboratories Materials Laboratory (AFWAL/MPO)

6c ADDRESS (City, State, and ZIP Code)	7b ADDRESS (City, State, and ZIP Code)
Stanford, CA 94305	Wright-Patterson Air Force Base, OH 45433-6533

8a NAME OF FUNDING/SPONSORING ORGANIZATION	8b OFFICE SYMBOL (If applicable)	9 PROCUREMENT INSTRUMENT IDENTIFICATION NUMBER
		F33615-84-C-5072

8c ADDRESS (City, State, and ZIP Code)	10 SOURCE OF FUNDING NUMBERS			
	PROGRAM ELEMENT NO	PROJECT NO	TASK NO	WORK UNIT ACCESSION NO
	62102F	2423	01	

11 TITLE (Include Security Classification) Modeling of Substrate and Implantation Effects on the Threshold Voltage of MESFET Structures Fabricated in Semi-Insulating GaAs

12 PERSONAL AUTHOR(S)
Thomas W. Sigma

13a TYPE OF REPORT	13b TIME COVERED	14 DATE OF REPORT (Year, Month, Day)	15 PAGE COUNT
Final	FROM 9/84 TO 5/86	December 1986	59

16 SUPPLEMENTARY NOTATION

17	COSATI CODES		18 SUBJECT TERMS (Continue on reverse if necessary and identify by block number)
FIELD	GROUP	SUB GROUP	Gallium Arsenide, MESFET, Process Modeling, Ion Implantation
9	1	21, 36	
20	12	5	

19 ABSTRACT (Continue on reverse if necessary and identify by block number)

The primary objective of this process modeling program was to identify Semi-Insulating Gallium Arsenide (SI-GaAs) substrate and implantation parameters that affect device behavior.

Three major areas were investigated.

1. Predicting the two-dimensional distribution of the EL2 anti-site defect.

2. Modeling changes in the two-dimensional EL2 distribution resulting from the annealing of Si-GaAs.

3. Determining the electrical characteristics of SI-GaAs substrate and the thermal stability of these characteristics.

(over)

20 DISTRIBUTION/AVAILABILITY OF ABSTRACT	21 ABSTRACT SECURITY CLASSIFICATION
☒ UNCLASSIFIED/UNLIMITED ☐ SAME AS RPT ☐ DTIC USERS	Unclassified

22a NAME OF RESPONSIBLE INDIVIDUAL	22b TELEPHONE (Include Area Code)	22c OFFICE SYMBOL
WILLIAM C. MITCHEL	(513)/255-6671	AFWAL/MLPO

DD Form 1473, JUN 86   Previous editions are obsolete   SECURITY CLASSIFICATION OF THIS PAGE

Unclassified

19. ABSTRACT (continued)

A two-dimensional computer model was developed to predict the thermally induced stress in a growing Czochralski GaAs boule from fundamental growth parameters. A "stress-conversion coefficient" was obtained from experimental data and was applied to the stress results to predict two-dimensional EL2 profiles. These predicted profiles were compared with experimental results.

A quasi-two-dimensional annealing computer model was constructed to model diffusion from calculated and experimental EL2 distributions. Experimental annealing data was used in the annealing model to obtain the approximate diffusion constant of the EL2 defect. This diffusion constant was then used in conjunction with the annealing model to predict the theoretical EL2 concentration before and after annealing. The predicted profiles were compared with experiment.

A Fermi-level computer model was constructed to determine the Fermi-level at each point in the wafer as a function of four arbitrary impurities. Once obtained, the Fermi level was used to calculate the resistivity at each location in the wafer. Theoretical results were calculated for unannealed material containing EL2, carbon, iron and silicon.

DTIC
COPY
INSPECTED
6

TABLE OF CONTENTS

TABLE OF CONTENTS (Concluded)

LIST OF FIGURES

I. REVIEW

The primary objective of this process modeling program was to identify Semi-Insulating Gallium Arsenide (SI-GaAs) substrate and implantation parameters that affect device behavior.

Three major areas were investigated.

1. Predicting the two-dimensional distribution of the EL2 anti-site defect.

2. Modeling changes in the two-dimensional EL2 distribution resulting from the annealing of SI-GaAs.

3. Determining the electrical characteristics of the SI-GaAs substrate and the thermal stability of these characteristics.

A two-dimensional computer model was developed to predict the thermally induced stress in a growing Czochralzki GaAs boule from fundamental growth parameters. A "stress-conversion coefficient" was obtained from experimental data and was applied to the stress results to predict two-dimensional EL2 profiles. These predicted profiles were compared with experimental results.

1

A quasi-two-dimensional annealing computer model was constructed to model diffusion from calculated and experimental EL2 distributions. Experimental annealing data was used in the annealing model to obtain the approximate diffusion constant of the EL2 defect. This diffusion constant was then used in conjunction with the annealing model to predict the theoretical EL2 concentration before and after annealing. The predicted profiles were compared with experiment.

A Fermi-level computer model was constructed to determine the Fermi-level at each point in the wafer as a function of four arbitrary impurities. Once obtained, the Fermi level was used to calculate the resistivity at each location in the wafer. Theoretical results were calculated for unannealed material containing EL2, carbon, iron and silicon.

II. BACKGROUND ON SI-LEC GaAs MATERIAL

1. Introduction

Semi-insulating Gallium Arsenide (SI-GaAs) substrates offer the advantages of device isolation, low interconnect capacitance, simplified processing, and direct ion-implantation for device fabrication. However, the quality and homogeneity of SI-GaAs material varies widely due to difficulties encountered during crystal growth. In order to achieve the tremendous advantages of GaAs technology, it is essential to understand the physical mechanisms behind the growth of the GaAs material.

2. Growth methods

Two major growth techniques (Horizontal Bridgeman and Liquid-Encapsulated-Czochralski) exist for producing SI-GaAs material. In the Horizontal Bridgeman (HB) method, the crystal is grown by zone-refining a GaAs melt in a quartz ampoule. The use of quartz introduces silicon as an impurity, requiring electrical compensation with chromium in order to maintain semi-insulating properties. Unfortunately, chromium tends to outdiffuse during thermal processing, causing the surface to change character from n to p type during thermal annealing. This thermally unstable behavior means that HB crystals are unacceptable for any annealed ion-implantation process [1].

In the Liquid-encapsulated-Czochralski (LEC) method, the crystal is grown by a Czochralski process incorporating an encapsulating blanket of boric oxide to maintain proper stoichometry. One major advantage of the SI-LEC growth process is that the material can be grown semi-insulating without intentional doping. The unintentional compensation mechanism responsible for the semi-insulating behavior of LEC-SI GaAs is believed to be EL2 deep donors compensating carbon shallow acceptors [2].

4

The major disadvantage of the SI-LEC process is the high dislocation density obtained during growth (ten to fifty times that of the HB process) [3]. The origin of these dislocations is not fully understood, but it appears to be related to abrupt temperature gradients occurring during growth. However, recent results on isoelectronic doping of SI-LEC material with gallium and indium show that impurity hardening by isoelectronic doping can greatly reduce the dislocation density without significantly changing the electrical properties [4,5]

3. The Unintentional Compensation of EL2 with Carbon

A crucial element in the growth of SI-LEC GaAs is the
unintentional compensation of the EL2 defect by carbon
impurities.

Carbon is probably introduced into the melt by the graphite
heaters used to heat the crucible.   Carbon (with a segregation
coefficient of approximately 2) is constant across each wafer
slice, but decreases from the seed to the tail of the boule [6].

EL2 (a deep level trap associated with the As/Ga anti-site
defect) increases from seed to tail in an As-rich boule,
decreases from seed to tail in a Ga-rich boule and is essentially
constant in a stoichiometric boule [7].   However, since EL2 is
associated with As on a Ga site, it is present only in very low
concentrations in Ga-rich boules.

The major concern with the EL2 defect is its variation in
the radial direction.   As can be seen in Figure 1,   the EL2
concentration displays a characteristic "W" shape when measured
across a diameter [8].   This is of great concern, because the
compensation between a constant carbon concentration and a "W"-
shaped EL2 concentration results in non-uniformity of electrical
parameters across a wafer [9].

$[EL2] \times 10^{15} cm^{-3}$

rho = 0

Normalized radius, $rho = r/r_0$
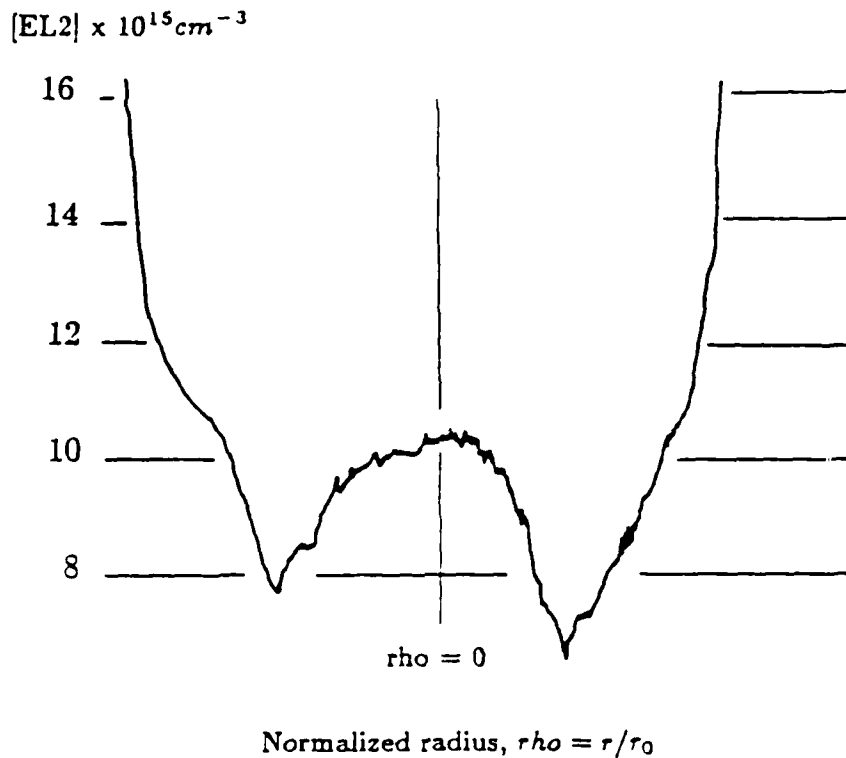
Figure 1 - EL2 Variation in the Radial Direction

The major concern with the EL2 defect is its variation in the radial direction. As can be seen above, the EL2 concentration displays a characteristic "W" shape when measured across a diameter. This is of great concern, because the compensation between a constant carbon concentration and a "W"-shaped EL2 concentration results in non-uniformity of electrical parameters across the wafer.

7

4. Summary

Clearly, the key technical issue in the growth of SI-LEC GaAs is the nature of the EL2 defect. Answers to the following questions are crucial to understanding the EL2 defect and its impact on device electrical performance. The remainder of this report will address some of these questions.

1. What is the physical mechanism which creates EL2?

2. Can the EL2 concentration profile be predicted from fundamental information?

3. What is the origin of the ubiquitous "W" shape for radial EL2 density profiles?

4. Can the "W" shaped EL2 concentration profile be made constant?

5. Does the compensation between the "W" shaped EL2 concentration and the constant carbon concentration result in variation in electrical parameters?

6. Is the compensation between EL2 and carbon thermally stable?

III. DETERMINING THE TWO-DIMENSIONAL DISTRIBUTION OF THE EL2 ANTI-SITE DEFECT.

1. Background - Identification and Evidence for the EL2 defect

Little was understood about the material growth of GaAs until 1981, when the materials groups at both Rockwell and Westinghouse began to seriously address the material problem.

These researchers discovered that extremely high quality undoped GaAs crystals could only be reproducibly grown from LEC material if the melt were maintained with an arsenic atomic fraction between 0.47 and 0.52. They also observed that high Hall mobility could only be maintained if the melt were slightly arsenic overrich. Finally, they noted that the tails of gallium rich boules underwent a transition from SI to p-type down the length of the boule, while arsenic rich boules did not display this property [10].

The conclusion was that a balance had been reached between shallow acceptors due to impurities and some sort of deep donor which was related to the arsenic concentration. A deep donor with this type of concentration dependent behavior is likely to be a point defect. If one assumes that the defect is a simple atomic disorder, then only an anti-site defect can account for the swing from p to n as the material becomes arsenic rich [11].

A big step in identifying the principle defect in GaAs material was taken by Martin et. al. In 1977, he had summarized all of the currently known defects in GaAs as measured by DLTS (Deep Level Transient Spectroscopy) as well as their cross-sections and activation energies [12]. In 1980, Martin et.al. used OTCS (Optical Transient Current Spectroscopy) to identify the deep donor they named EL2, with an activation energy of about 0.784 eV, and was identified with a characteristic optical absorption fingerprint between 1 and 1.4 microns. [13]

At this point in time (1981), the conclusion was that an anti-site defect existed in the high-quality SI material, and that it was compensating some impurity (probably carbon) resulting from the LEC process.

Before considering the nature of this compensation process it is important to ask a more fundamental question. Is this EL2 defect a process dependent effect that will be eliminated in the next few years by better growth methods for GaAs? Although it is likely that better methods will be developed to grow GaAs material, a vast body of information exists for Czochalski growth for silicon. Although better growth techniques may be developed, from an engineering and economy standpoint LEC material may always be the material of choice.

2. Origin of the EL2 defect

In 1984, Holmes et.al. [14] measured two-dimensional dislocation density profiles and observed a correlation between dislocation density and EL2 concentration. This correlation had been observed before, but only in one-dimensional cross-section [15-17].

In 1980, Jordan et.al. [18] analyzed two-dimensional thermal stress profiles in a growing Czochralski boule and observed a correlation between thermal stress and dislocation density. Since 1980, several studies have verified this correlation between theoretical stress profiles and experimentally measured dislocation densities [19-21].

Clearly, if thermal stress correlates to dislocation density, and dislocation density correlates to EL2 concentration, then thermal stress correlates to EL2 concentration.

The KEY question is if thermal stress is LINKED to EL2 concentration. This possibility was first suggested by Martin et. al. in 1981 [22]. Evidence for this link was provided by Weber et.al. (1982) when he measured the creation of EL2 defect during plastic deformation of GaAs [23].

11

A variety of mechanisms have been proposed to account for the stress induced production of EL2 in GaAs. These mechanisms fall into three principle categories:

1. Stress forms dislocations, and dislocations create EL2
2. Stress forms EL2, and EL2 condenses into dislocations
3. EL2 and dislocations are independent

In 1981, Parsey et.al. showed that it is possible to grow dislocation-free material with an EL2 concentration comparable to conventional material [24]. This result suggests that dislocations do not create EL2.

In 1981, Chen et.al. showed that dislocations always increase from seed to tail in a CZ-LEC GaAs crystal, but that EL2 concentration depends on the stoichometry [25]. This suggests that EL2 condensing into dislocations is not the principle mechanism for the formation of dislocations.

This evidence suggests that stress produces dislocations and the EL2 defect, but that the two processes are independent. Thus, prediction of the stress induced during growth of the GaAs boule could be used to predict the EL2 concentration.

12

3. **Mathematical analysis of stress in a growing Czochralski boule.**

The system being modeled is a GaAs boule during Czochralski growth. (See Figure 2) The key item being calculated is the thermal stress induced in the boule as a result of the growth process. (Note that this is NOT the residual stress contained in the boule after the boule is removed from the melt and cooled) The key assumption is that the EL2 defect is formed during the growth process at the time when the thermal stress is maximized.

Jordan's 1979 paper [26] contains a careful analysis of heat conduction and thermal stress during Czochralski growth. The key equations from this paper are summarized in the following few pages. (Note: In order to increase the usefulness of this summary, the derivation is presented backwards; the answer preceeds the fundamental equations used to obtain it.)
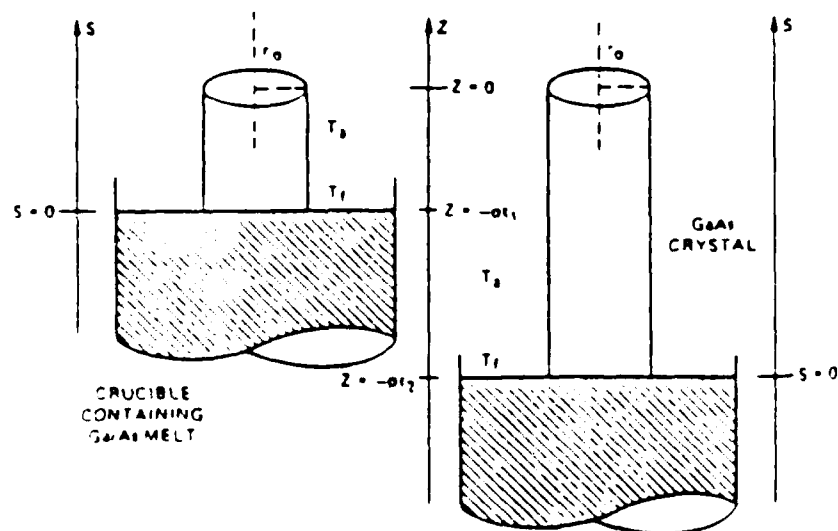
Figure 2 - Czochralski Growth of a GaAs Boule

The system being modeled is a GaAs boule during Czochralski growth. The key item being calculated is the thermal stress induced in the boule as a result of the growth process. (Note that this is NOT the residual stress contained in the boule after the boule is removed from the melt and cooled) The key assumption is that the EL2 defect is formed during the growth process at the time that the thermal stress is maximized.

14

Initially, a few boule specific parameters must be obtained:

κ = THERMAL CONDUCTIVITY (WATT/CM K),

r = EVALUATION RADIUS (CM) r_0 = BOULE RADIUS (CM)

θ = EVALUATION ANGLE (RADIANS) T = PULL TIME (SECONDS)

p = PULL RATE (CM/SECOND) h = HEAT TRANSFER (1/CM)

s = z+pt = EVALUATION LOCATION (CM) E = YOUNG'S MODULUS (DYNES/CM2)

α = EXPANSION COEFFICIENT (1/K) ν = POISSON'S RATIO

T = BOULE TEMPERATURE (K) T_a = AMBIENT TEMPERATURE (K)

T_f = MELT TEMPERATURE (K) ϵ = EMISSIVITY

l = BORIC OXIDE THICKNESS (CM) P = PRESSURE (DYNES/CM2)

In order to simplify analysis, the following additional terms are defined from the fundamental information:

$$h_1 = h r_0$$

$$p_1 = \frac{p r_0}{\kappa}$$

$$h_p = \frac{p_1}{2} + h_1$$

$$\rho = \frac{r}{r_0}$$

$$\Psi = \frac{z + pt}{r_0}$$

$$\Psi_t = \frac{pt}{r_0}$$

$$\beta_n = \left(\alpha_n^2 + \frac{p_1^2}{4} \right)^{1/2}$$

$$-\alpha_n J_1(\alpha_n) + h_1 J_0(\alpha_n) = 0$$

$$\overline{\sigma_r} = \sigma_r - \sigma_\theta$$

$$\overline{\sigma_z} = \sigma_z - \sigma_\theta$$

$$S_{cc} = 2h \frac{\alpha E}{1 - \nu} (T_f - T_a) \exp^{p_1 \Psi/2} r_0$$

15

Assuming that the stresses are mostly elastic, the total stress at a given (rho, theta) location in a GaAs wafer can be expressed as the sum of the stresses along all slip planes.

$$\sigma_{tot} = 4|\sigma_I| + 2|\sigma_{II}| + 2|\sigma_{III}| + 2|\sigma_{IV}| + 2|\sigma_V|$$

In the GaAs system (analyzed quasi-isotropically), there are twelve possible slip planes. Five of these slip planes are independent. The stresses on these five independent slip planes can be expressed as follows:

direction/plane

[-110] / (111)
[110] / (-111) $\sigma_I = -\dfrac{\sqrt{6}}{6}\overline{\sigma_r}\cos 2\theta$
[1-10] / (-1-11)
[-1-10] / (1-11)

[0-11] / (111) $\sigma_{II} = \dfrac{\sqrt{6}}{6}\left[\overline{\sigma_z} - \overline{\sigma_r}\dfrac{2}{\sqrt{2}}\sin\theta\sin\left(\theta + \dfrac{\pi}{4}\right)\right]$
[011] / (-1-11)

[0-11] / (-111) $\sigma_{III} = \dfrac{\sqrt{6}}{6}\left[\overline{\sigma_z} - \overline{\sigma_r}\dfrac{2}{\sqrt{2}}\sin\theta\sin\left(\theta - \dfrac{\pi}{4}\right)\right]$
[011] / (1-11)

[10-1] / (111) $\sigma_{IV} = -\dfrac{\sqrt{6}}{6}\left[\overline{\sigma_z} - \overline{\sigma_r}\dfrac{2}{\sqrt{2}}\cos\theta\sin\left(\theta + \dfrac{\pi}{4}\right)\right]$
[-10-1] / (-1-11)

[-10-1] / (1-11) $\sigma_V = -\dfrac{\sqrt{6}}{6}\left[\overline{\sigma_z} + \overline{\sigma_r}\dfrac{2}{\sqrt{2}}\cos\theta\sin\left(\theta - \dfrac{\pi}{4}\right)\right]$
[10-1] / (1-11)

Where, in these equations the following alternative radial and axial stress terms have been used:

$$\overline{\sigma_r} = \sigma_r - \sigma_\theta$$

$$\overline{\sigma_z} = \sigma_z - \sigma_\theta$$

The radial, angular and axial stress terms contained in the alternative stress terms can be obtained from:

$$\sigma_r = S_{cc} \sum_{n=1}^{\infty} \left(\frac{h_p \sinh \beta_n (\Psi_t - \Psi) + \beta_n \cosh \beta_n (\Psi_t - \Psi)}{(h_1^2 + \alpha_n^2) J_0 (\alpha_n) (h_p \sinh \beta_n \Psi_t + \beta_n \cosh \beta_n \Psi_t)} \right)$$

$$\cdot \left[\frac{J_1 (\alpha_n)}{\alpha_n} - \frac{J_1 (\alpha_n \rho)}{\alpha_n \rho} \right]$$

$$\sigma_\theta = S_{cc} \sum_{n=1}^{\infty} \left(\frac{h_p \sinh \beta_n (\Psi_t - \Psi) + \beta_n \cosh \beta_n (\Psi_t - \Psi)}{(h_1^2 + \alpha_n^2) J_0 (\alpha_n) (h_p \sinh \beta_n \Psi_t + \beta_n \cosh \beta_n \Psi_t)} \right)$$

$$\cdot \left[\frac{J_1 (\alpha_n)}{\alpha_n} + \frac{J_1 (\alpha_n \rho)}{\alpha_n \rho} - J_0 (\alpha_n \rho) \right]$$

$$\sigma_z = S_{cc} \nu \sum_{n=1}^{\infty} \left(\frac{h_p \sinh \beta_n (\Psi_t - \Psi) + \beta_n \cosh \beta_n (\Psi_t - \Psi)}{(h_1^2 + \alpha_n^2) J_0 (\alpha_n) (h_p \sinh \beta_n \Psi_t + \beta_n \cosh \beta_n \Psi_t)} \right)$$

$$\cdot \left[\frac{2 J_1 (\alpha_n)}{\alpha_n} - J_0 (\alpha_n \rho) \right]$$

17

Where Scc is given by:

$$S_{cc} = 2h\frac{\alpha E}{1-\nu}\left(T_f - T_a\right)\exp^{p_1\Psi/2} r_0$$

There are two possible solutions for the thermal stress in the growing boule. The previous solution results from the assumption of zero axial strain on the growing boule. However, if zero axial force is assumed, then the final solution differs in the axial stress term. The axial stress term for zero axial force is given by:

$$\sigma_z = S_{cc}\sum_{n=1}^{\infty}\left(\frac{h_p\sinh\beta_n\left(\Psi_t - \Psi\right) + \beta_n\cosh\beta_n\left(\Psi_t - \Psi\right)}{\left(h_1^2 + \alpha_n^2\right)J_0\left(\alpha_n\right)\left(h_p\sinh\beta_n\Psi_t + \beta_n\cosh\beta_n\Psi_t\right)}\right)$$

$$\cdot\left[\frac{2J_1\left(\alpha_n\right)}{\alpha_n} - J_0\left(\alpha_n p\right)\right]$$

It is still unclear which of the two assumptions (zero axial strain, or zero axial force) is the better model of the growing Czochralski boule.

18

All of the terms in the equations on the previous page are known material parameters EXCEPT for the terms alpha and beta. Beta is a function of alpha, defined by:

$$\beta_n = \left(\alpha_n^2 + \frac{p_1^2}{4} \right)^{1/2}$$

However, alpha must be obtained from the characteristic equation:

$$-\alpha_n J_1(\alpha_n) + h_1 J_0(\alpha_n) = 0$$

The radial, angular and axial stress terms detailed previously are derived by substituting the temperature profile for the growing boule into the fundamental integral stress equations for cylindrical geometry. The fundamental integral stress equations (assuming zero axial strain) are:

$$\sigma_r = \frac{aE}{1-r} \left(\frac{1}{r_0^2} \int_0^{r_0} Tr \, dr - \frac{1}{r^2} \int_0^r Tr \, dr \right)$$

$$\sigma_\theta = \frac{aE}{1-r} \left(\frac{1}{r_0^2} \int_0^{r_0} Tr \, dr + \frac{1}{r^2} \int_0^r Tr \, dr - T \right)$$

$$\sigma_z = \frac{aE}{1-r} \left(\frac{2\nu}{r_0^2} \int_0^{r_0} Tr \, dr - T \right).$$

19

With the assumption of zero axial force, the integral equation for the axial stress becomes:

$$\sigma_z = \frac{aE}{1-r} \left(\frac{2}{r_o^2} \int_0^{r_o} Tr \, dr - T \right)$$

The temperature profile required in the integral stress equations is derived from the fundamental heat conduction equation for a cylindrical geometry.

$$\frac{\partial T}{\partial t} = \kappa \left(\frac{\partial^2 T}{\partial r^2} + \frac{1}{r} \frac{\partial T}{\partial r} + \frac{\partial^2 T}{\partial z^2} \right)$$

This fundamental heat conduction equation can be simplified into the quasi-steady state form, and written with the dimensionless terms rho, eta and psi:

$$\frac{\partial^2 T}{\partial \rho^2} + \frac{1}{\mu} \frac{\partial T}{\partial \rho} + \frac{\partial^2 T}{\partial \psi^2} = p_1 \frac{\partial T}{\partial \psi}$$

The following product function can be used to separate the variables:

$$T = e^{p_1 \psi / 2} R(\rho) \Psi(\psi)$$

20

Yielding the separated differential equation:

$$\frac{d^2R}{Rd\rho^2} + \frac{1}{\rho R}\frac{dR}{d\rho} = \frac{p_1^2}{4} - \frac{1}{\Psi}\frac{d^2\Psi}{d\psi^2} = -\alpha^2$$

The R differential equation is:

$$\frac{d^2R}{d(\alpha\rho)^2} + \frac{dR}{\alpha\rho\, d\alpha\rho} + R = 0$$

With the solution:

$$R(\rho) = J_0(\alpha\rho)$$

The axial differential equation is:

$$\beta^2\Psi - \frac{d^2\Psi}{d\psi^2} = 0$$

With the solution:

$$\Psi = A \sinh \beta(\psi_t - \psi) + B \cosh \beta(\psi_t - \psi)$$

So, the final solution to the cylindrical quasi-steady state thermal conduction equation is:

$$T = T_a + e^{p_1\psi/2} \sum_{n=1}^{\infty} J_0(\alpha_n\rho) \frac{B_n}{\beta_n} [h_p\sinh \beta_n(\psi_l - \psi)$$

$$+ \beta_n\cosh \beta_n(\psi_l - \psi)].$$

The boundary conditions for the growing boule are:

$$\frac{\partial T}{\partial \psi} + h_1(T - T_a)|_{\psi=\psi_r} = 0$$

$$\frac{\partial T}{\partial s} + h(T - T_n)|_{s=\rho\epsilon} = 0$$

These can be applied to the solution of the cylindrical quasi-steady state thermal conduction equation, to yield:

$$\frac{dJ_n}{d\rho} (\alpha_n\rho) + h_1 J_0(\alpha_n\rho)|_{\rho=1} = 0$$

Applying the Bessel function recursion relation:

$$\frac{dJ_0(x)}{dx} = -J_1(x)$$

22

to the previous equation, results in the Bessel function characteristic equation which we showed previously.

$$-\alpha_n J_1(\alpha_n) + h_1 J_0(\alpha_n) = 0$$

4. Behaviour of the Stress in a Growing CZ-LEC Boule

Several of the growth parameters are key to understanding the behaviour of the growing Czochralski boule. These are:

h = The heat transfer coefficient between the boule and the ambient environment

ro = The radius of the boule

p = The growth rate of the boule

t = The time to grow the boule

s = z + pt = the distance from the melt interface to the location where the stress is being calculated.

"h" governs the heat transfer between the surface of the boule and the ambient environment. (Less heat transfer -- smaller "h") Intuitively, we would expect reduced stress for reduced heat transfer, so reducing "h" should reduce the stress. This intuitive conclusion is supported by Figure 3, where the normalized stress is compared for h = 1.8 and h = 0.6. (The zero axial strain solution is assumed, and other parameters are held constant at: p=1.94e-4 cm/sec, t=51546 sec, r=3.81 cm, s=1.5 cm and theta = 0.785 radians)

"ro" is the radius of the final boule. Intuitively, we would expect that the smaller the boule, the greater the stress involved during growth. This is borne out by Figure 4, which

compares the normalized stress at theta = .785 for ro = 2.54 cm (2" diameter boule) and ro = 3.81 (3" diameter boule). (The zero axial strain solution is assumed, and other parameters are held constant at: p=1.94e-4 cm/sec, t=51546 sec, h = 0.6, s=1.5 cm and theta = 0.785 radians)

"p" is the pull rate and "t" is the amount of time it takes to pull the boule. Intuitively, we would expect that the longer it takes to pull the boule the less the stress will be. This is true, as Figure 5 shows, but the effect is not as significant as might be expected. (The zero axial strain solution is assumed, and the other parameters are held constant at a constant length of 10 cm: h = 0.6, ro = 3.81 cm, s=1.0 cm and theta = 0.785 radians)

"s" is the distance from the melt/boule interface to the location where the stress will be computed. Clearly, as this distance increases, the stress will drop. This intuitive conclusion is borne out by the results in Figure 6, where the normalized stress is compared as a function of "s". (The zero axial strain solution is assumed, and the other parameters are held constant at: h = 0.6, ro = 3.81 cm, p=1.94e-4, t=51546, and theta = 0.785 radians)

Mathematically, the only difference between the zero axial strain and the zero axial force boundary conditions is a factor of Poisson's ratio in the axial stress equation. However, the total stress results differ significantly depending on the chosen assumption. Total stress results are shown in Figure 7 for both the zero axial strain and the zero axial force assumptions. Note that the assumption of zero axial force results in greater overall stresses, as well as a stress minimum placed at a greater distance from the wafer center than the zero axial strain assumption.

COMPARISON OF h FACTORS
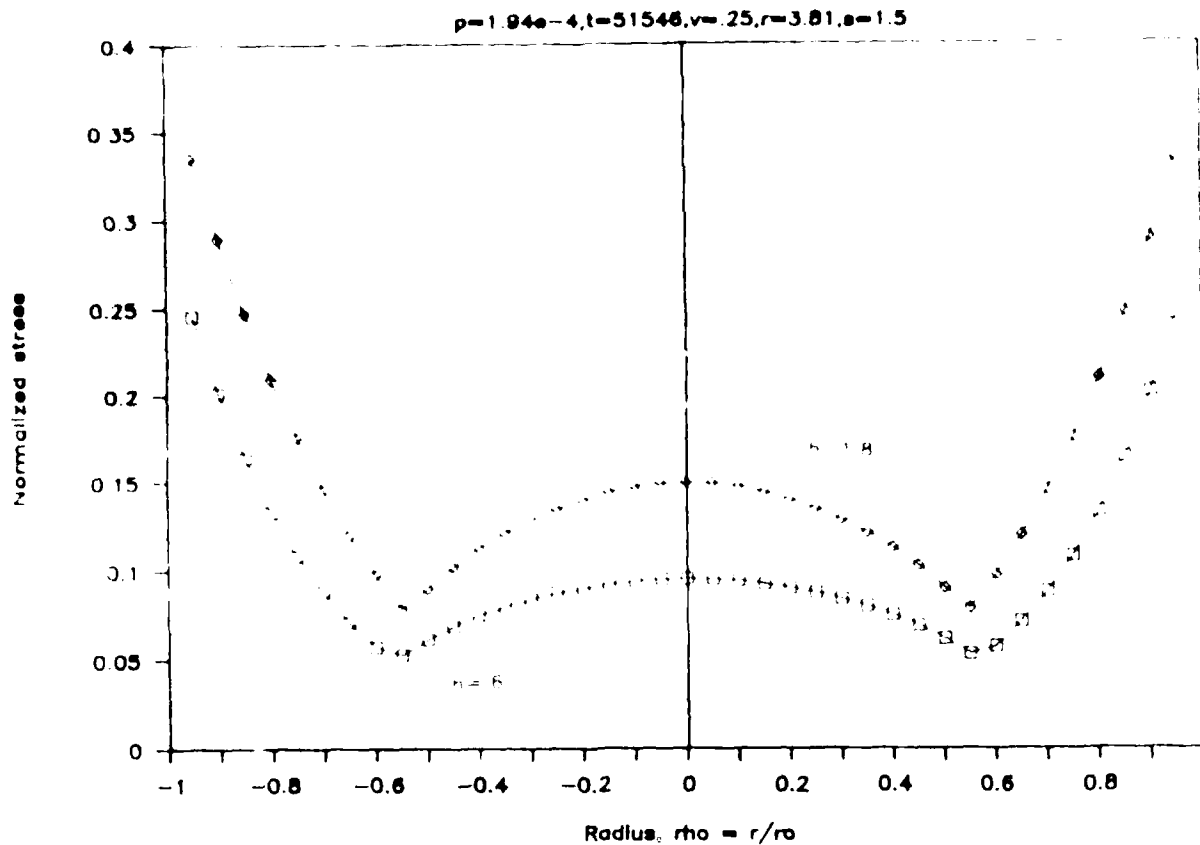### p=1.94e-4,t=51546,v=.25,r=3.81,s=1.5

Figure 3 - Comparison of "h" factors

"h" governs the heat transfer between the surface of the boule
and the ambient environment. (Less heat transfer -- smaller "h")
Intuitively, we would expect reduced stress for reduced heat
transfer, so reducing "h" should reduce the stress. This
intuitive conclusion is supported by the above graph, where the
normalized stress is compared for h = 1.8 and h = 0.6. (The zero
axial strain solution is assumed, and other parameters are held
constant at: p=1.94e-4 cm/sec, t=51546 sec, r=3.81 cm, s=1.5,
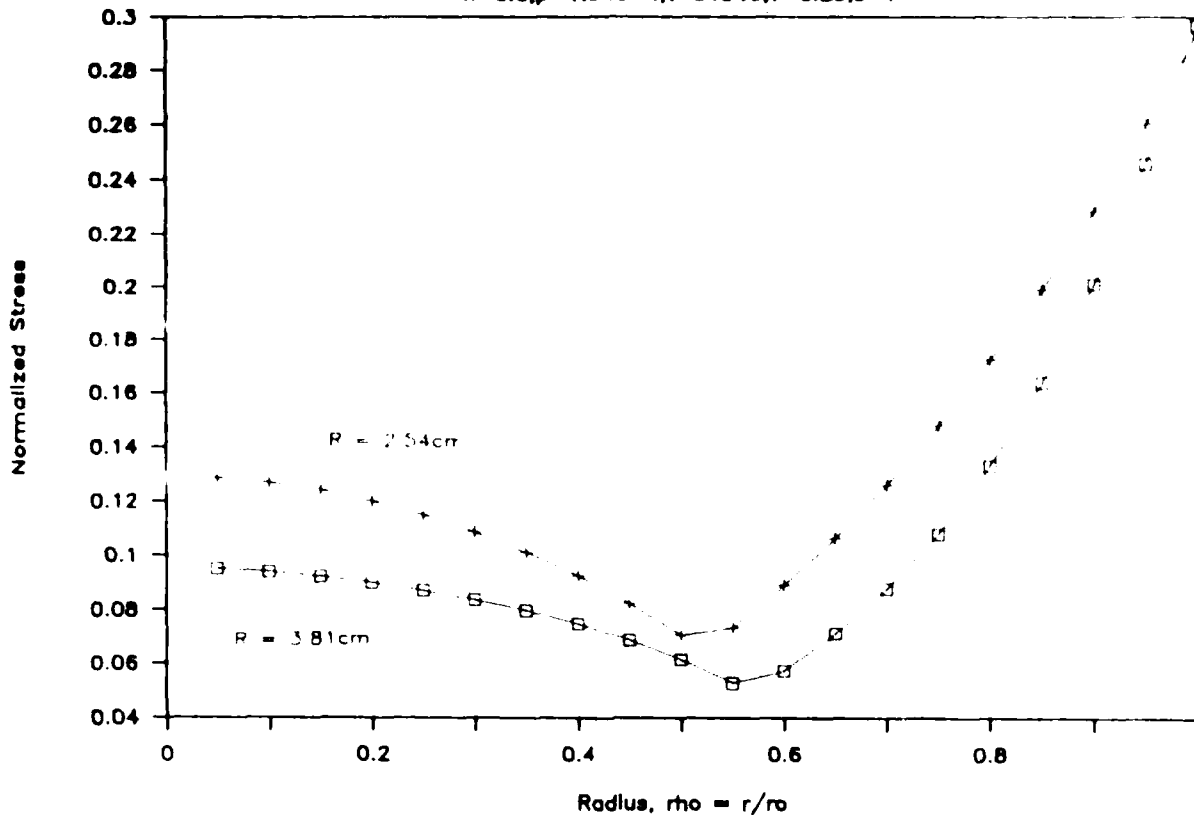and theta = 0.785 radians)

EFFECT OF BOULE DIAMETER

Figure 4 - Effect of Boule Diameter

"ro" is the radius of the final boule. Intuitively, we would expect that the smaller the boule, the greater the stress involved during growth. This is borne out by the above graph which compares the normalized stress at theta = .785 for ro = 2.54 cm (2" diameter boule) and ro = 3.81 (3" diameter boule). The zero axial strain solution is assumed, and other parameters are held constant at: p=1.94e-4 cm/sec, t=51546 sec, h = 0.6, s=1.5 cm and theta = 0.785 radians)

28

EFFECT OF PULL RATE AND TIME
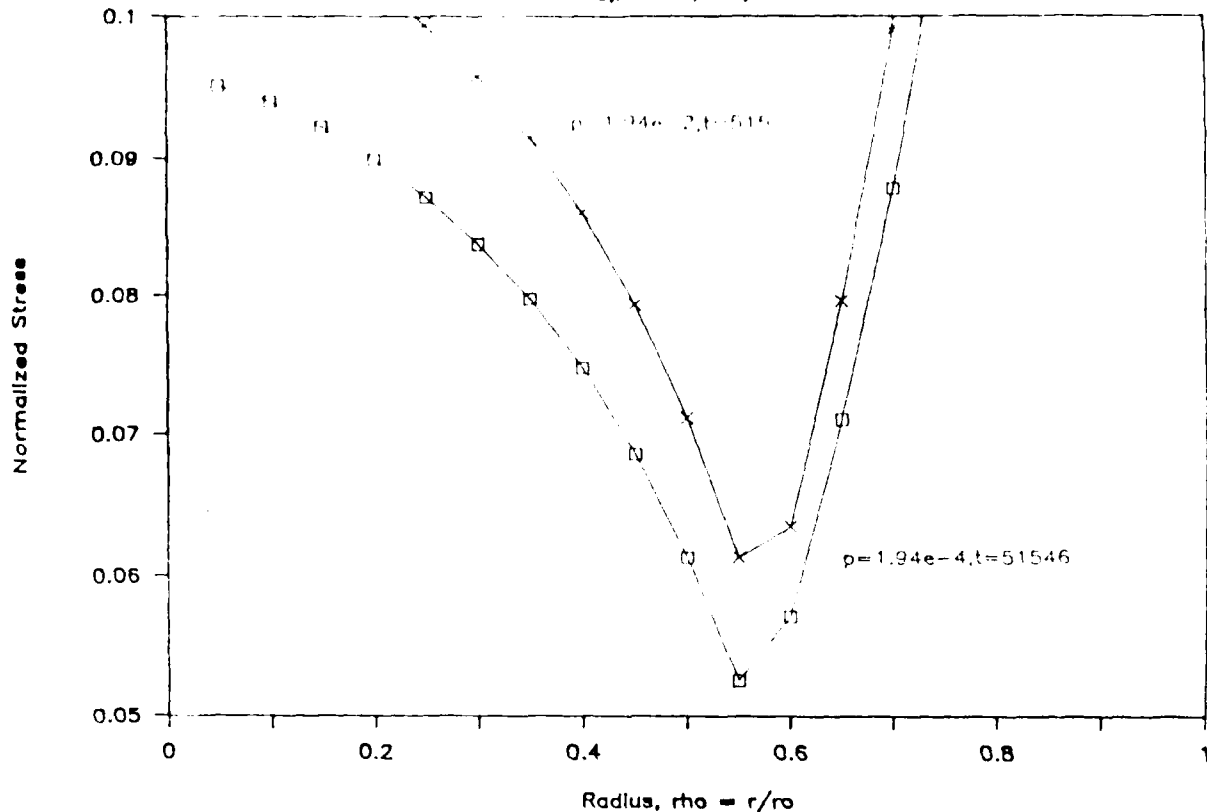
h=.6,r=3.81,s=1,v=.25

Figure 5 - Effect of Pull Rate and Time

"p" is the pull rate and "t" is the amount of time it takes to pull the boule. Intuitively, we would expect that the longer it takes to pull the boule the less the stress will be. This is true, as Figure 5 shows, but the effect is not as significant as might be expected. (The zero axial strain solution is assumed, and the other parameters are held constant at a constant length of 10 cm: h = 0.6, ro = 3.81 cm, s=1.0 cm and theta = 0.785 radians)

29

EFFECT OF MELT/BOULE DISTANCE
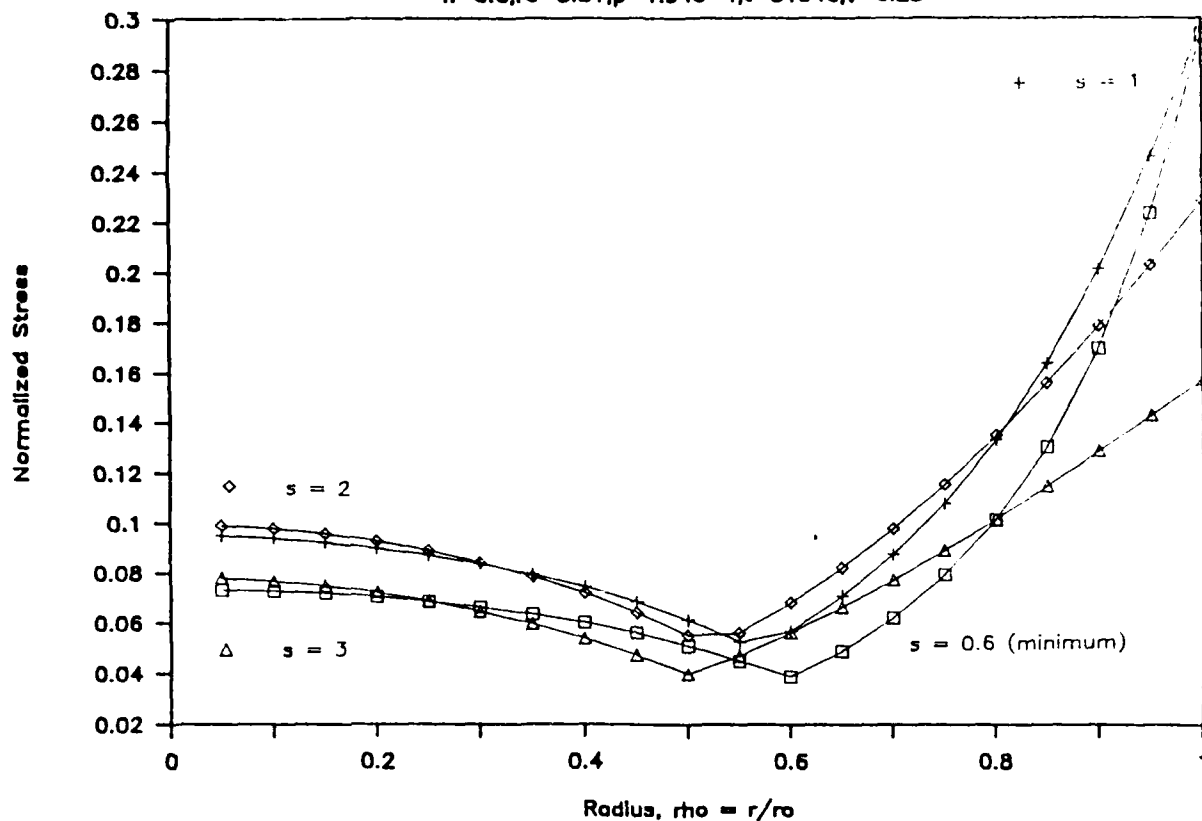### h=0.6,ro=3.81,p=1.94e−4,t=51546,v=0.25

Figure 6 – Effect of Melt/Boule Interface Distance

"s" is the distance from the melt/boule interface to the location where the stress will be computed. Clearly, as this distance increases, the stress will drop. This intuitive conclusion is borne out by the above graph, where the normalized stress is compared as a function of "s". (The zero axial strain solution is assumed, and the other parameters are held constant at: h = 0.6, ro = 3.81 cm, p=1.94e-4 cm/sec, t=51546 sec, s = 1 cm and theta = 0.785 radians)

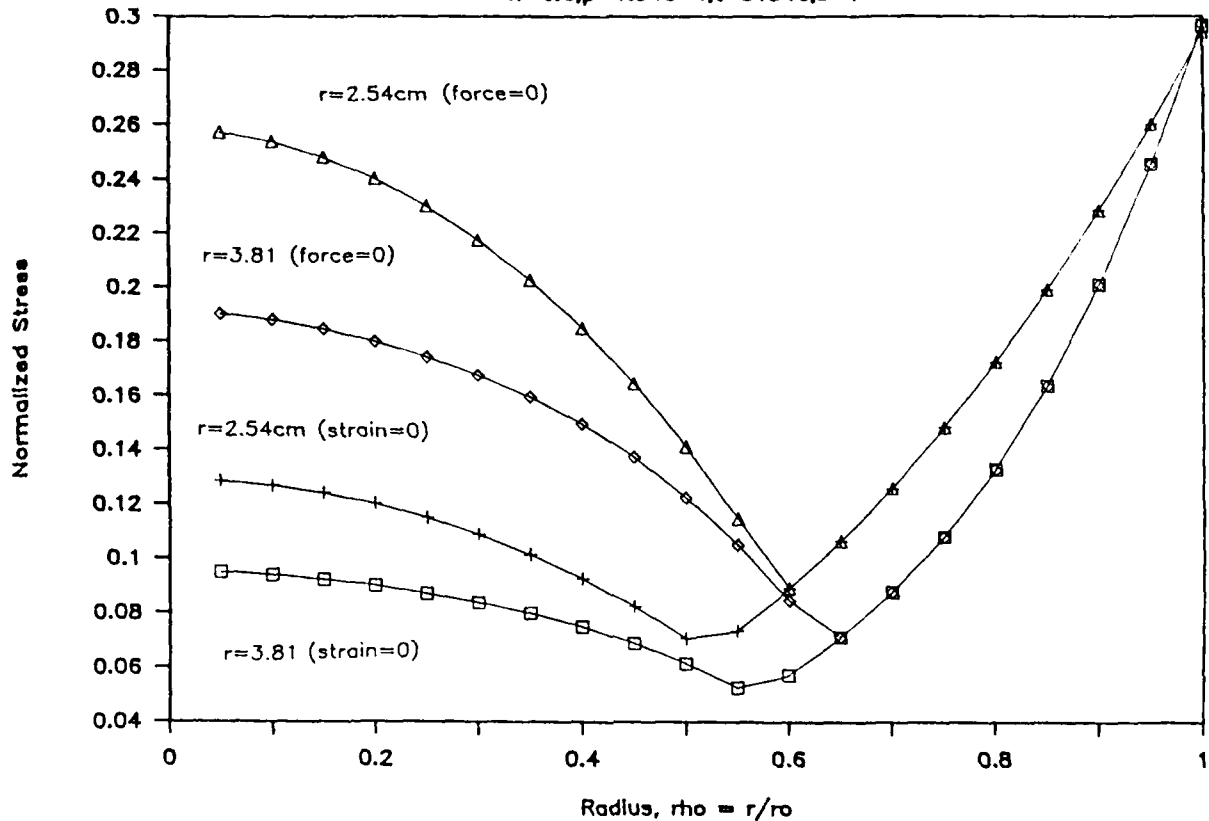## ZERO AXIAL STRAIN V.S. ZERO AXIAL FORCE

h=0.6,p=1.94e-4,t=51546,s=1

Figure 7 - Zero Axial Force versus Zero Axial Strain

Mathematically, the only difference between the zero axial strain and the zero axial force boundary conditions is a factor of Poisson's ratio in the axial stress equation. However, the total stress results differ significantly depending on the chosen assumption. Total stress results are shown above for both the zero axial strain and the zero axial force assumptions. Note that the assumption of zero axial force results in greater overall stresses, as well as a stress minimum placed at a greater distance from the wafer center than the zero axial strain assumption. (The other parameters are held constant at: h = 0.6, ro = 3.81 cm, p=1.94e-4 cm/sec, t=51546 sec, s = 1 cm and theta = 0.785 radians)

5. Obtaining the stress conversion coefficient

Jordan's equations are usually solved for a "normalized-stress" which differs from the actual stress by a factor Scc (see previous). Ideally, the EL2 concentration should be obtained by multiplying this normalized stress by a factor Mcc which consists of the product of Scc and the stress-conversion-coefficient. This factor Mcc is constant for all boules grown with identical temperature distributions and boric oxide thicknesses, (the radii and pull rates may differ). Note that this method of EL2 calculation does not require knowledge of the values of T, Ta and Tf. This is advantageous since these temperatures are difficult to measure experimentally.

We empirically determined Mcc by using a computer model (developed from Jordan's stress equations) to compare theoretical stress values (both for the assumption of zero axial strain and of zero axial force) with experimental results from Brozel et.al. [27]. The results of this comparison are shown in Figure 8. The zero axial strain assumption yields a better match between theory and experiment with an empirically determined value for Mcc obtained from this comparison is 9e16 [EL2]/cm4.

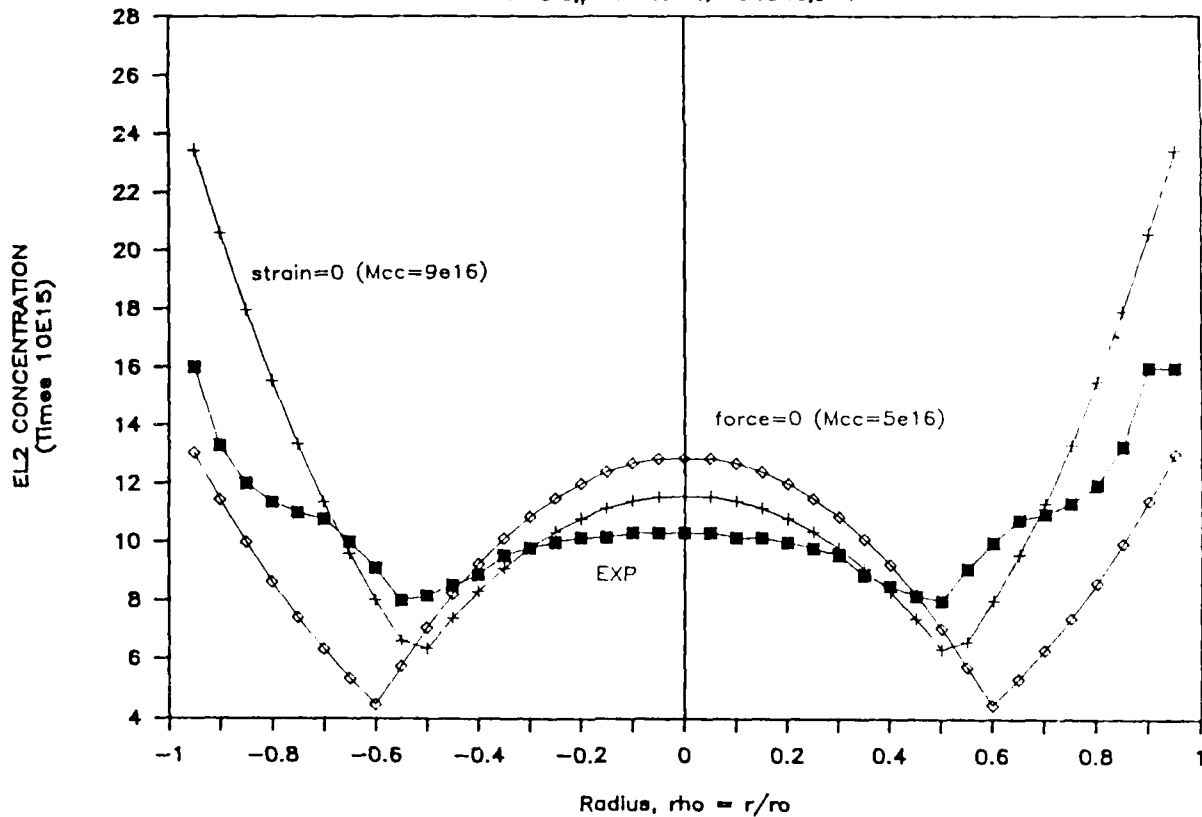## THEORY VERSUS EXPERIMENT (BROZEL)

h=0.6,p=1.94e-4,t=51546,s=1

Figure 8 - Obtaining the Stress Conversion Coefficient

We empirically determined Mcc by using a computer model (developed from Jordan's stress equations) to compare theoretical stress values (both for the assumption of zero axial strain and of zero axial force) with experimental results from Brozel et.al. [27]. The results of this comparison are shown in Figure 8. The zero axial strain assumption yields a better match between theory and experiment with an empirically determined value for Mcc obtained from this comparison is 9e16 [EL2]/cm4. (The other parameters are held constant at: h = 0.6, ro = 3.81 cm, p=1.94e-4 cm/sec, t=51546 sec, s = 1 cm and theta = 0.785 radians)

33

6. Predicting the two-dimensional EL2 distribution

Once the "stress-conversion-coefficient" is known, it is possible to predict two-dimensional EL2 concentration profiles using the previously described equations. We developed a computer model capable of calculating the EL2 distributions from fundamental material parameters. Figure 9 shows a comparison between the predicted EL2 profiles (for both the zero axial strain and the zero axial force assumptions) and experimental profiles (measured by Holmes). Figures 10 and 11 show detailed views of the predicted EL2 profiles for each axial assumption.
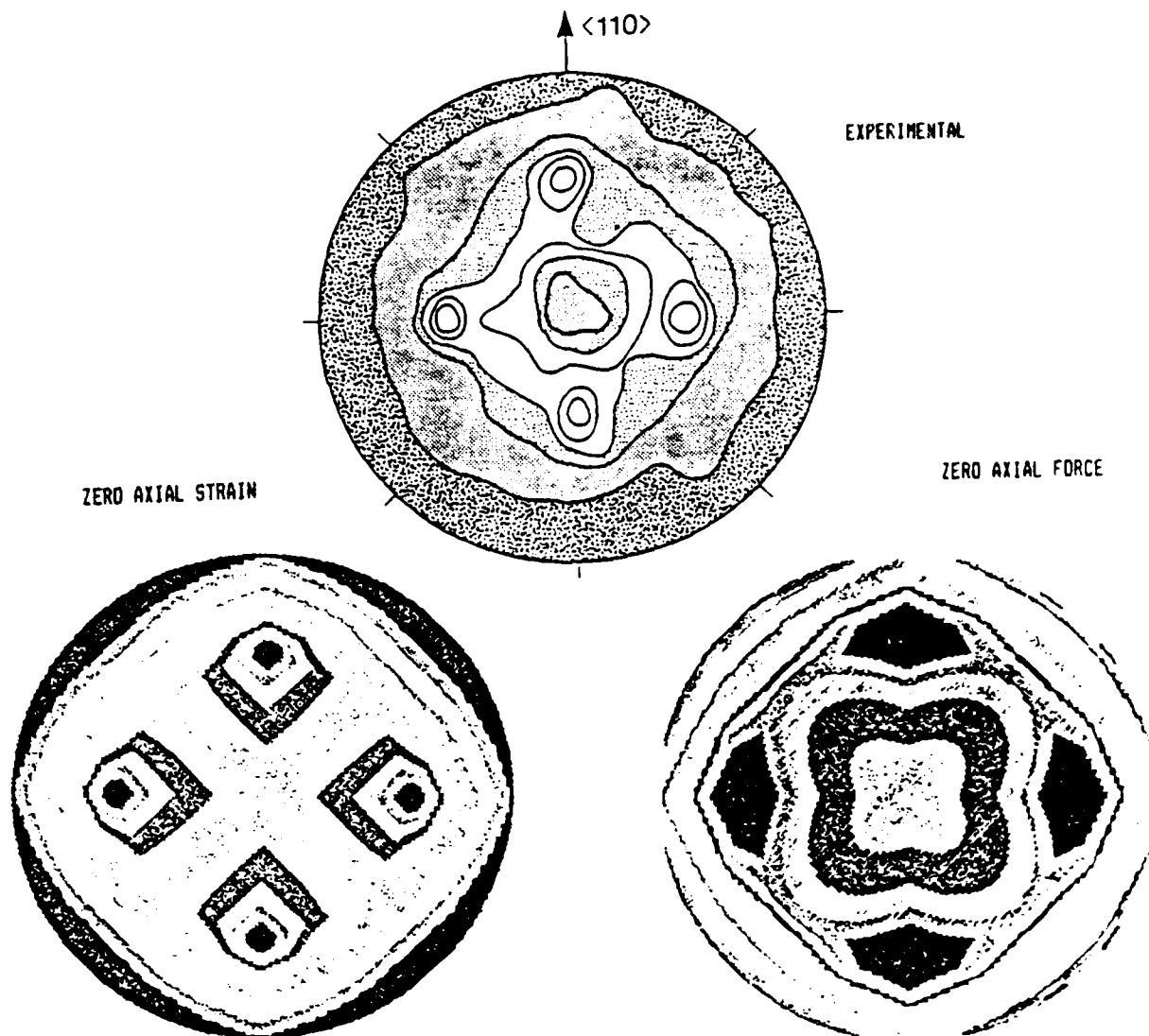
Figure 9 - Two Dimensional EL2 Concentration Profiles

Once the "stress-conversion-coefficient" is known, it is possible to predict two-dimensional EL2 concentration profiles using the previously described equations. We developed a computer model capable of calculating the EL2 distributions from fundamental material parameters. The above figure shows a comparison between the predicted EL2 profiles (using both the zero axial stress and zero axial strain assumptions) and experimental profiles (measured by Holmes). (The other parameters are held constant at: h = 0.6, ro = 3.81 cm, p=1.94e-4 cm/sec, t=51546 sec, s = 1 cm and theta = 0.785 radians)

35

Figure 10 - The Zero Axial Strain Assumption

The above figure shows a detailed view of the EL2 concentration
profile resulting from using the zero axial strain assumption.
(The other parameters are held constant at: h = 0.6, ro = 3.81 cm,
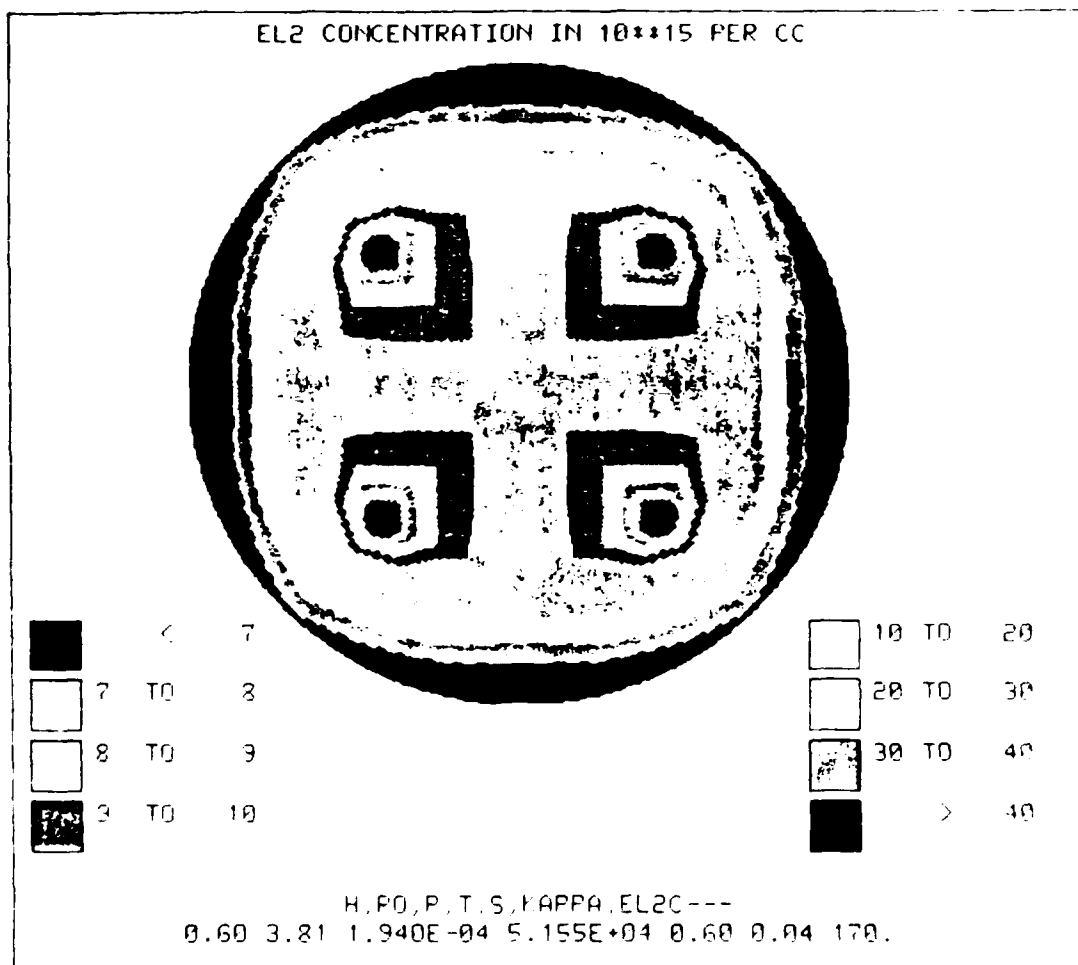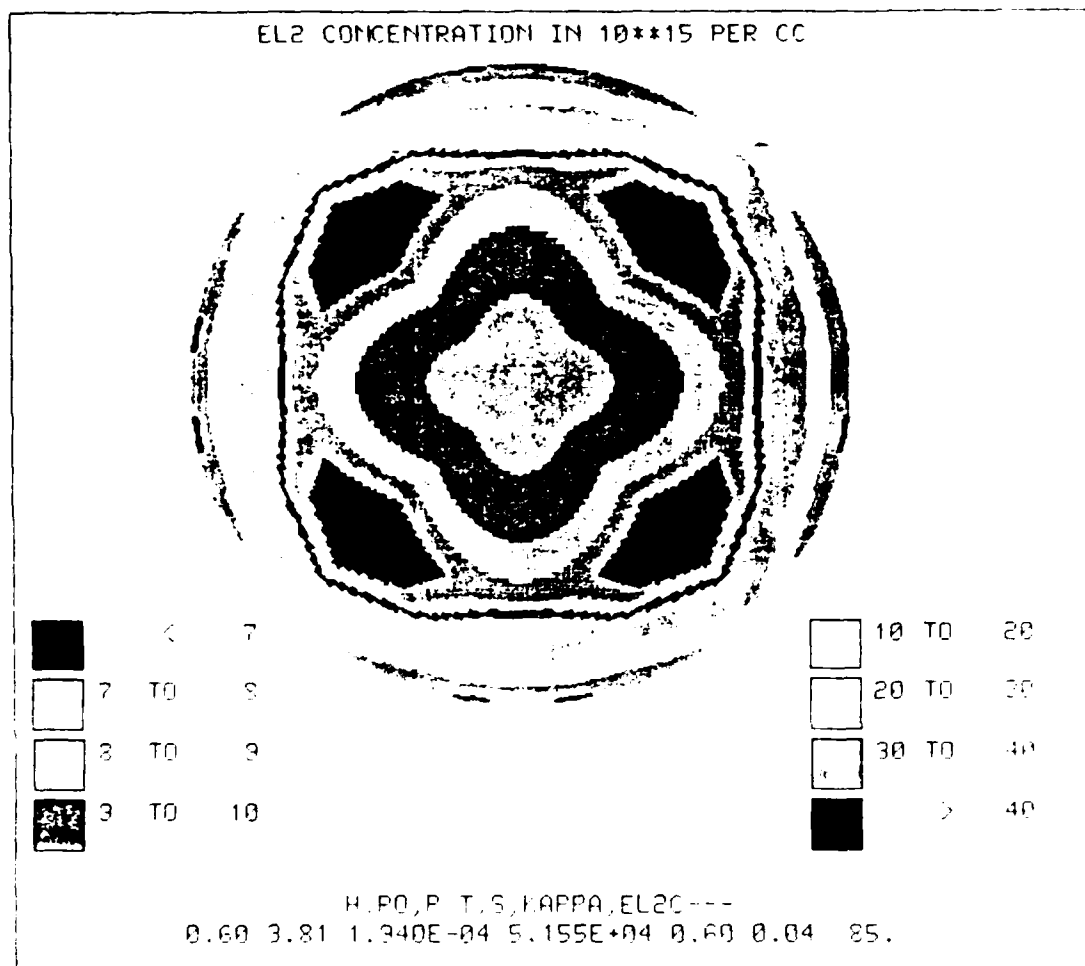p=1.94e-4 cm/sec, t=51546 sec, s = 0.6 cm and theta = 0.785
radians)

36

Figure 11 - The Zero Axial Force Assumption

The above figure shows a detailed view of the EL2 concentration profile resulting from using the zero axial force assumption. (The other parameters are held constant at: h = 0.6, ro = 3.81 cm, p=1.94e-4 cm/sec, t=51546 sec, s = 0.6 cm and theta = 0.785 radians)

37

IV. ANNEALING THE EL2 DEFECT

1. Introduction

The critical step in fabricating an ion-implanted MESFET device is the activation anneal. It is vitally important that the electrical characteristics of the GaAs substrate not change during the activation anneal.

We developed a quasi-two-dimensional computer model to simulate the effects of an activation anneal on the EL2 defect profile. This model takes the theoretical EL2 defect density and performs a one-dimensional Gaussian diffusion at each calculated point in the substrate.

Initially, the approximate diffusion coefficient for the EL2 defect in GaAs was determined by taking existing experimental results and curve-fitting them to the results of the computer model. Once the diffusion coefficient was obtained, it was used in conjunction with the computer model to predict EL2 defect density profiles before and after annealing.

2. Initial Observation of Annealing

A comparison between theory and experiment was performed using data from Holmes [28]. The results of this comparison for both the zero axial strain and zero axial force assumptions (using the multiplicative coefficient of 1.9 e17 [EL2]/cm^4) are shown in Figure 12. Although the overall agreement between theory and experiment is quite good for the zero axial strain assumption, the edges do deviate considerably from theory.

We postulated that this deviation was due to a post-growth annealing process occurring as a result of the boule cooling in the puller for many hours. We therefore expanded the computer model to take theoretical EL2 concentrations (as predicted by the stress calculations) and diffuse these throughout the boule.

COMPARISON OF THEORY TO EXPERIMENT

p=1.94e-4,t=51546,r=3.81,s=1

Figure 12 - Comparison of Theory with Experiment (Holmes)
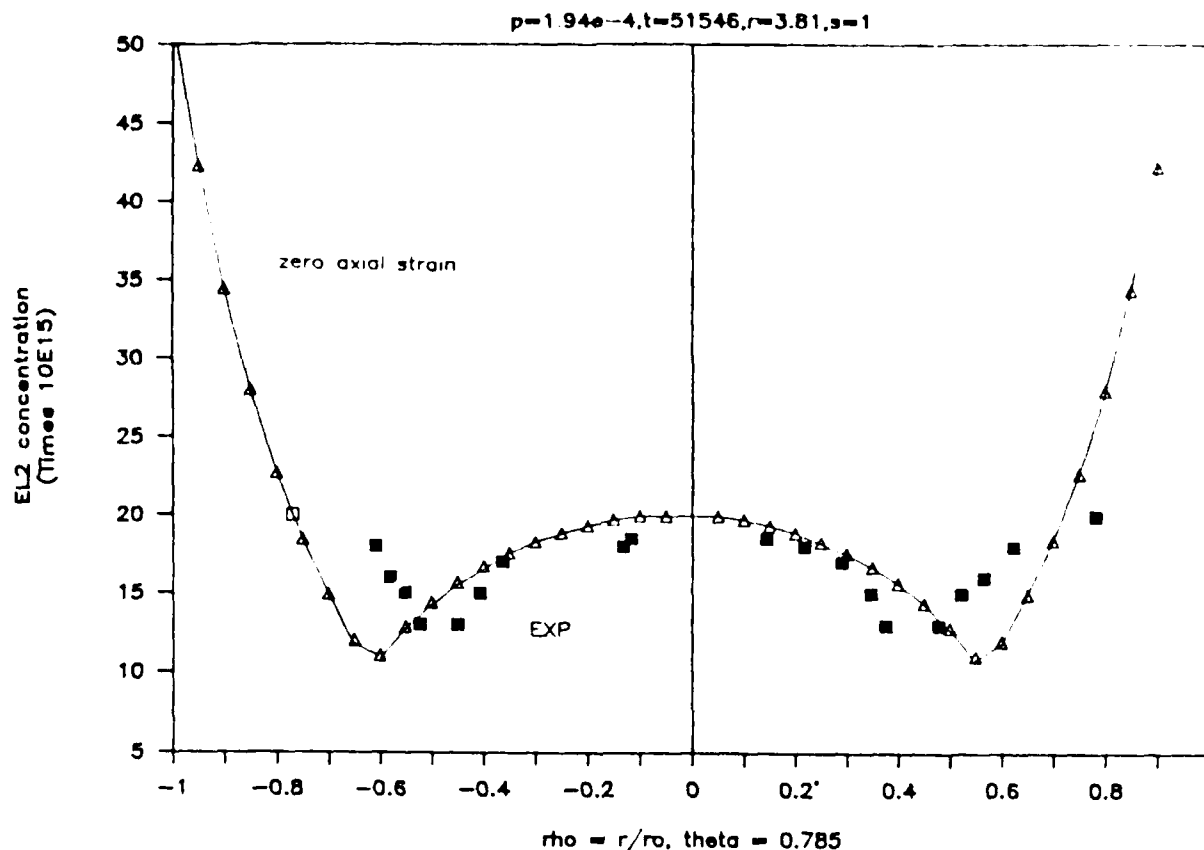
A comparison between theory and experiment was performed using data from Holmes [28]. The zero axial strain assumption yields a good correlation between theory and experiment with an empirically determined value for Mcc of 1.9e16 [EL2]/cm4. (The other parameters are held constant at: h = 0.6, ro = 3.81 cm, p=1.94e-4 cm/sec, t=51546 sec, s = 1 cm and theta = 0.785 radians)

3. Determination of the Approximate Diffusion Coefficient

Figure 9 shows experimental annealing results from Holmes
[24]. Using our annealing model, we roughly evaluated the
diffusion constant of EL2 at 950 C by comparing theoretically
calculated annealed profiles against the actual annealed
profiles. These calculations result in a diffusion constant
of 7 (+- 5) e-7 cm2/sec.

The value obtained for this diffusion constant is quite
high. The magnitude of this value suggests that EL2 is diffusing
by an interstitial mechanism as opposed to a substitional
mechanism. This, in turn, suggests that some part of the
mechanism responsible for generating EL2 may be based on an
interstitial defect.

These annealing results suggest the following model.
During Czochralski growth, thermal stresses cause modifications
of the electric field in the ionic GaAs crystal. These field
modifications create charged sites attractive to excess
interstitial arsenic atoms. During annealing, the excess
interstitial arsenics become more mobile, and migrate to other
charged sites in the crystal.

41

EXPERIMENTAL RESULTS FROM
LONG-TERM ANNEALING

(Experimental Results from Holmes)

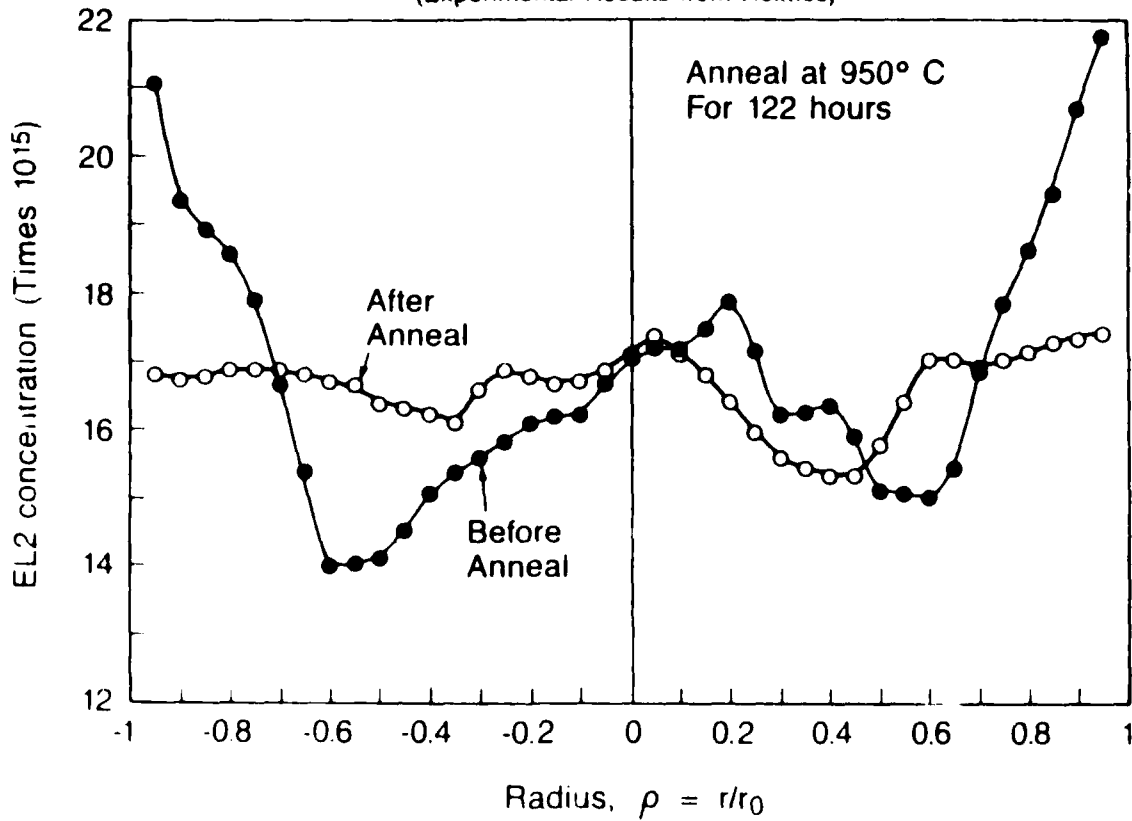Figure 13 - Annealing the EL2 Defect (Holmes)

This graph shows experimental results from Holmes obtained from annealing the EL2 defect in GaAs [24]. Using our annealing model, we roughly evaluated the diffusion constant of EL2 at 950 C by comparing theoretically calculated annealed profiles against the actual annealed profiles. These calculations result in a diffusion constant of 7 (+- 5) e-7 cm2/sec.

4. Comparison of the Annealing Model with Experiment

As we mentioned earlier, we postulated that the difference in curve shape between the theoretical results and Holmes's experimental results was due to a post-growth annealing process occurring as a result of the boule cooling in the puller for many hours. Using this assumption, as well as assuming outdiffusion from the GaAs boule, we recalculated the EL2 distribution.

Figures 14 compares the diffused EL2 results with the experimental values. The correlation between the diffused EL2 results and the actual experimental values (from Holmes) is quite good. This suggests that post-growth whole-boule anneal may alter the EL2 concentration results as obtained from stress calculations. It also suggests that post-growth whole-boule anneal may be a way to equalize EL2 concentration across the boule.

ANNEALING THE EL2 DEFECT

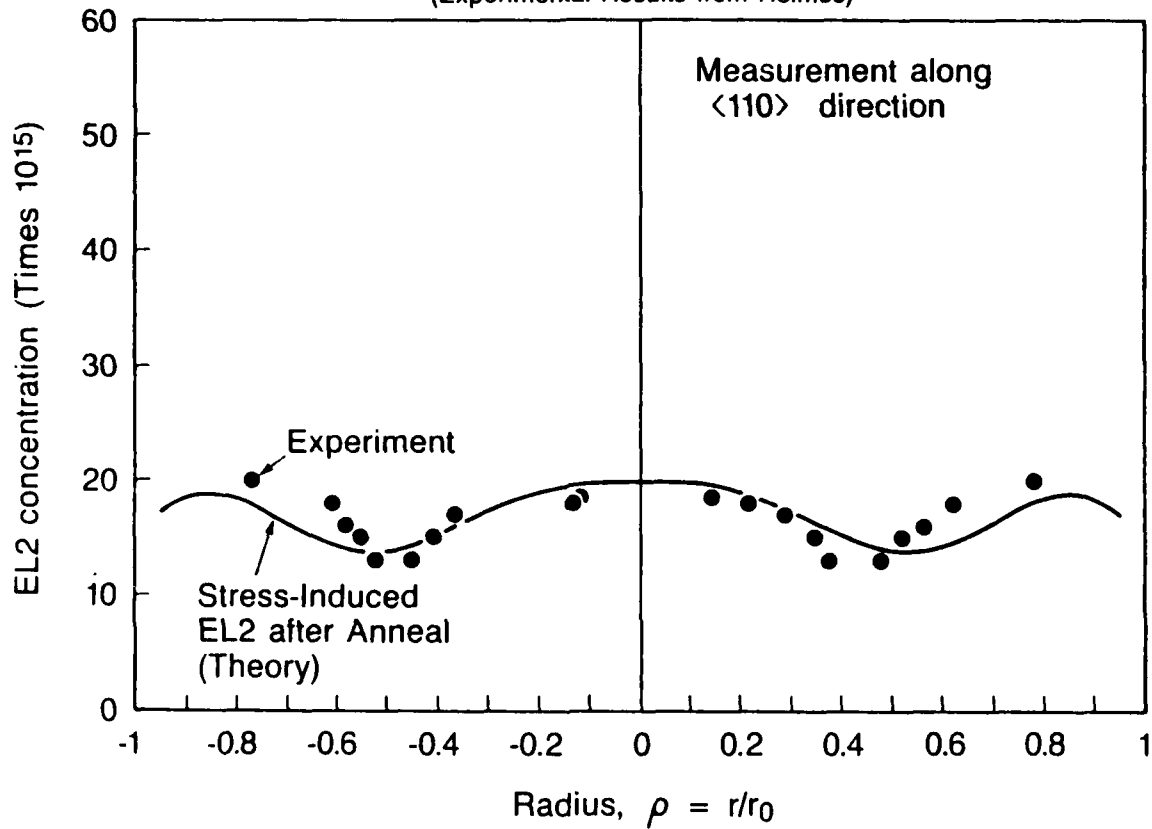### (Experimental Results from Holmes)

Figure 14 - Comparison of annealed and unannealed results for
the EL2 defect

This graph compares the diffused EL2 results (obtained from the
annealing model as applied to the stress analysis) with the
experimental values from Holmes.

44

V. ELECTRICAL CHARACTERISTICS OF THE SI-GaAs SUBSTRATE AND THE THERMAL STABILITY OF THESE CHARACTERISTICS

1. Introduction

Clearly, the variation of the EL2 defect across the substrate is unimportant if it does not affect device performance. Since substrate resistivity is of primary concern in an ion-implanted device, our first objective was to predict the resistivity at each location on the wafer as a function of the EL2 concentration.

A Fermi-level computer model was constructed to calculate the Fermi-level at each point in the wafer as a function of four arbitrary impurities. Once obtained, the Fermi level was then used to calculate the resistivity at each location in the wafer. Theoretical results were obtained for unannealed material containing EL2, carbon, iron and silicon.

45

2. Theory of the Fermi-level Analysis

There are a variety of impurities and defects in SI-LEC material (see Figure 15). The most important are carbon (acceptor), iron (acceptor), EL2 (donor) and silicon (donor).

The relative concentrations and energies of these various impurities determines the location of the Fermi-level in the bandgap. Once calculated, the location of the Fermi-level in the gap can be used to obtain many other electrical properties of interest (resistivity, and trap-filled limit voltage for example).

The charge neutrality condition for a substrate containing four major impurity levels is:

$$n + N_{A-iron}^{(-)} + N_{A-carbon}^{(-)} = p + N_{D-EL2}^{(+)} + N_{D-silicon}^{(+)}$$

The electron and hole density (n and p) are given in terms of the Fermi-level as:

$$n = N_c exp\left(\frac{-(E_c - E_f)}{kT}\right)$$

$$p = N_v exp\left(\frac{-(E_f - E_v)}{kT}\right)$$

46
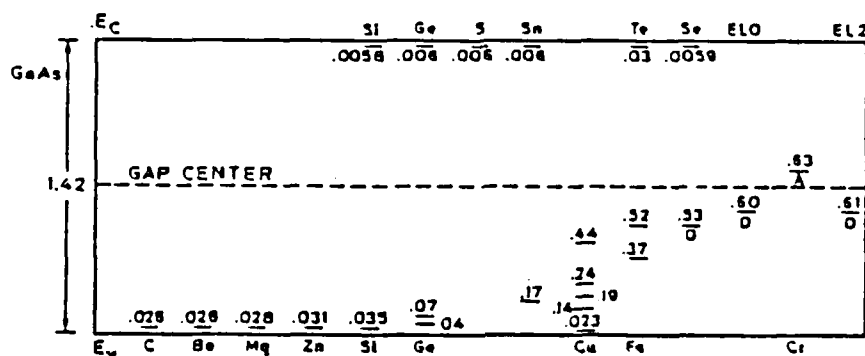
Figure 15 - Summary of Defects and Impurities in GaAs

There are a variety of impurities and defects in SI-LEC material.
the most important are carbon (acceptor), iron (acceptor), EL2
(donor) and silicon (donor). The relative concentrations and
energies of these various impurities determines the location of
the Fermi-level in the bandgap. Once calculated, the location
of the Fermi-level in the gap can be used to obtain many other
electrical properties of interest (resistivity, and trap-filled
limit voltage for example).

47

The concentrations of the various defects and impurities are also given in terms of the Fermi-level as:

$$N_A^- = \frac{N_A}{1 + g \exp\left(\frac{E_A - E_F}{kT}\right)}$$

$$N_D^+ = N_D \left[1 - \frac{1}{1 + \frac{1}{g} \exp\left(\frac{E_D - E_F}{kT}\right)} \right]$$

The concentrations of carbon, iron and silicon are essentially constant across an SI-LEC wafer. Unfortunately, the EL2 concentration displays a characteristic W pattern. This means that the Fermi-level must be recalculated for each point on the wafer.

Once the Fermi-level is determined for each point, then it can be used to calculate various electrical parameters of interest at that point. For example, the electron and hole densities (n and p) can be calculated from the Fermi-level:

$$n = N_c exp\left(\frac{-(E_c - E_f)}{kT}\right)$$

$$p = N_v exp\left(\frac{-(E_f - E_v)}{kT}\right)$$

These can then be used to determine the resistivity on a point by point basis.

$$\rho = \frac{1}{q(\mu_n n + \mu_p p)}$$

3. Calculation for a Wafer

Holmes's data [30] was selected for an initial computation of the Fermi-level and resistivity in a real system. The characteristics of the boule and wafer are:

1. Boule pull time = 51546 seconds
2. Boule pull rate = 1.94 e-4 cm/sec
3. Assumed Mcc = 1.7 el7 [EL2]/cm4
4. Carbon = 6 el5 [C]/cm3
5. Iron = 3 el5 [Fe]/cm3
6. Silicon = 2 el5 [Si]/cm3

First, the computer model was run with these values to create a database containing the EL2 concentration as a function of location. Then, the Fermi-level and resistivity were calculated. These results are shown in Figures 16-17.

Figure 16 - Computation of the Fermi-level

This graph shows an initial computation of the Fermi-level in a
real system. The system parameters are: Boule pull time = 51546
seconds, Boule pull rate = 1.94 e-4 cm/sec, h = 0.6, s = 1 cm, r
= 3.81 cm, assumed Mcc = 1.7 e17 [EL2]/cm4, Carbon = 6 e15
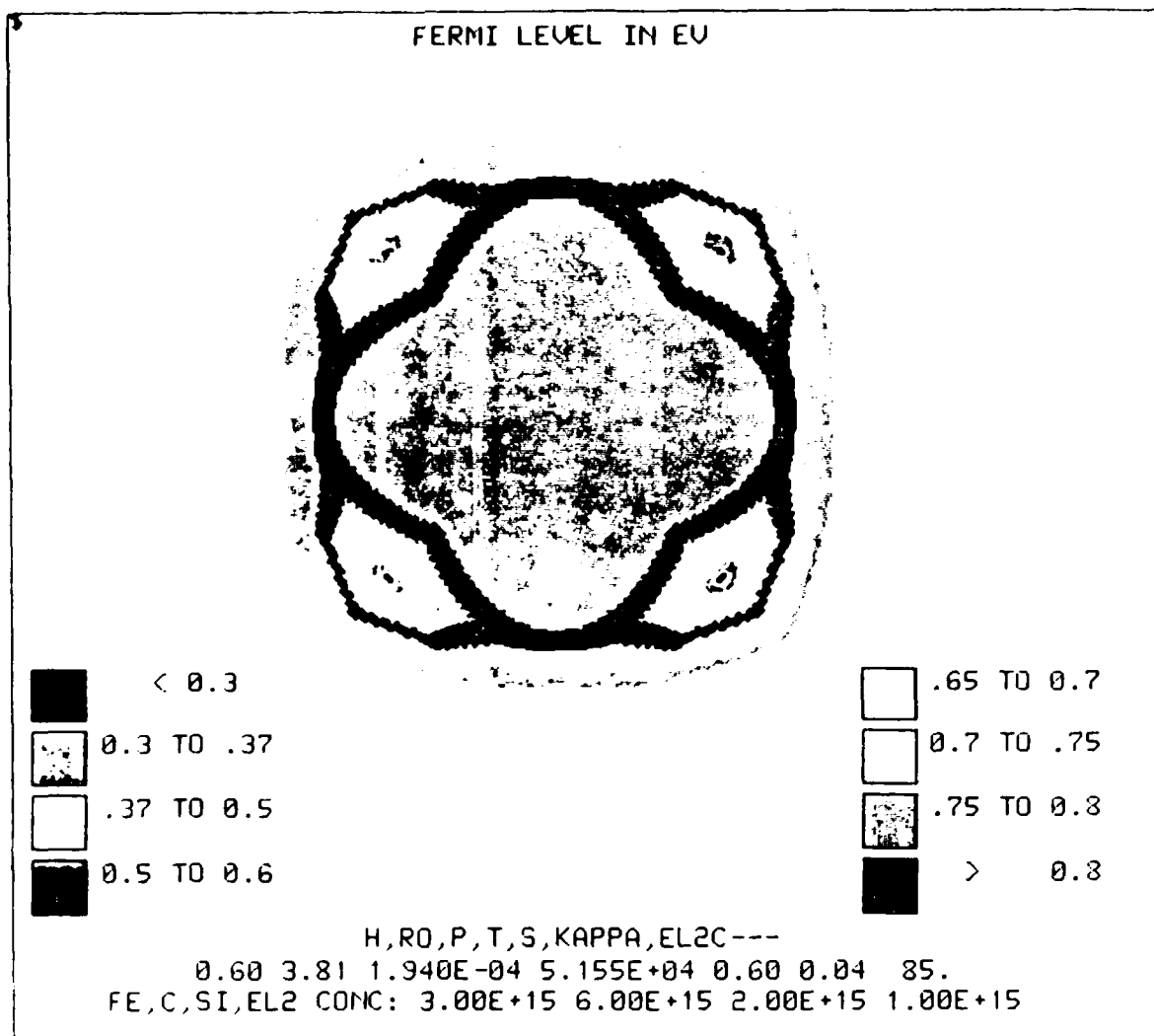[C]/cm3, Iron = 3 e15 [Fe]/cm3 and Silicon = 2e15 [Si]/cm3.
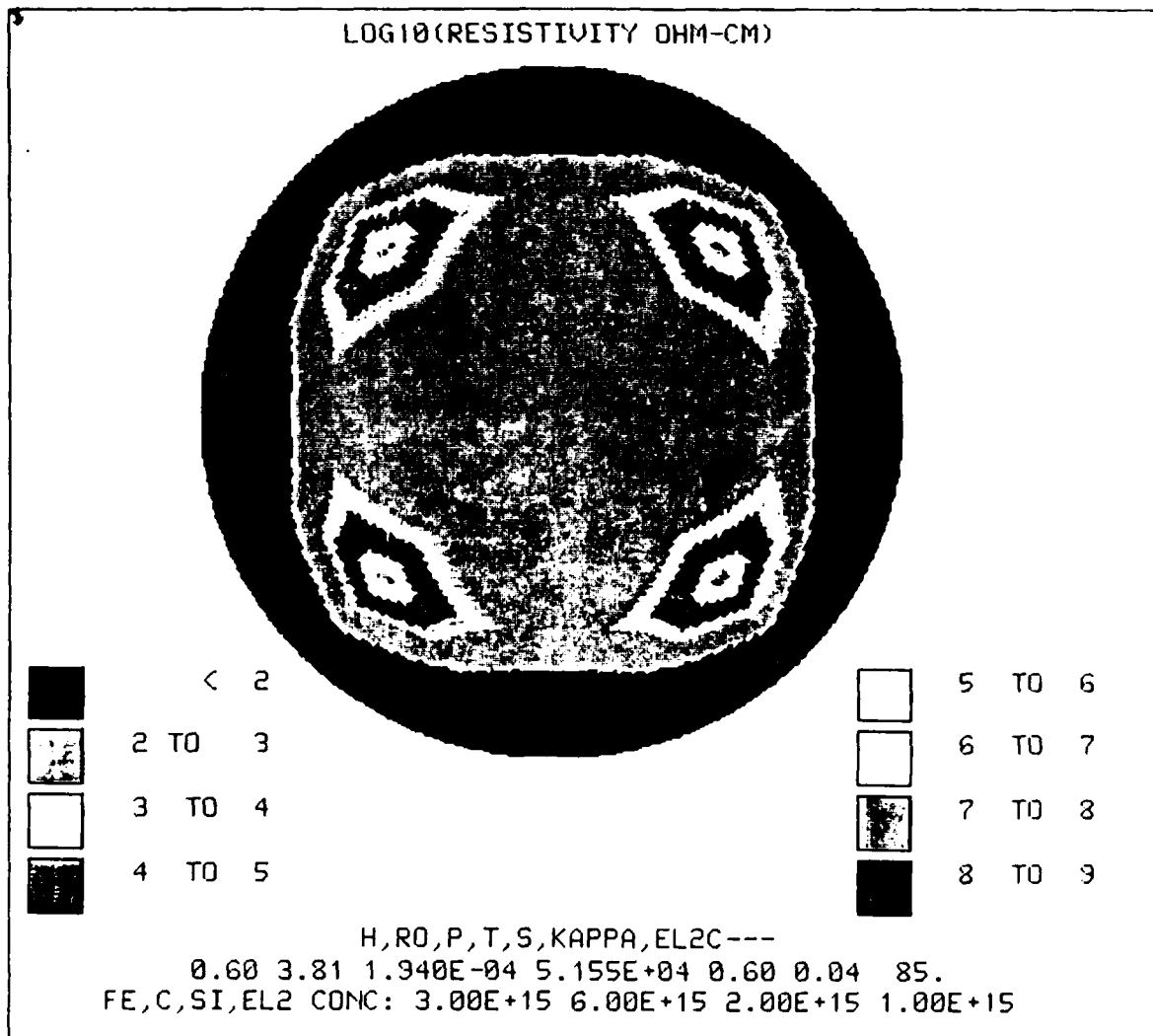
Figure 17 - Computation of the Resistivity

This graph shows an initial computation of the resistivity in a real system. The system parameters are: Boule pull time = 51546 seconds, Boule pull rate = 1.94 e-4 cm/sec, h = 0.6, s = 1 cm, r = 3.81 cm, assumed Mcc = 1.7 el7 [EL2]/cm4, Carbon = 6 el5 [C]/cm3, Iron = 3 el5 [Fe]/cm3 and Silicon = 2 el5 [Si]/cm3.

4. Summary

The previous results are extremely interesting. As we might expect, the extremes of the EL2 concentration curve display the greatest deviation in Fermi-level and resistivity. What this means is that an improvement in the uniformity of the EL2 distribution results in an improvement in the uniformity of the substrate resistivity. Since annealing improves the uniformity of the EL2 distribution, it is clear that the quality of the GaAs substrate can be improved by whole-boule post-growth annealing.

VI. CONCLUSIONS

The key technical issue in the growth of SI-LEC material is understanding and controlling the EL2 anti-site defect. With the results from this project in mind, answers can be proposed to the six questions introduced earlier in this report:

1. What is the physical mechanism which creates EL2?

> The evidence strongly suggests that thermal stress occurring during growth of the Czochralski boule creates EL2. EL2 distributions can be accurately predicted by calculating the theoretical stress and applying a simple multiplicative "stress-conversion-coefficient".

2. Can the EL2 concentration profile be predicted from fundamental information?

> The EL2 concentration profiles can be predicted by applying a "stress-conversion-coefficient" to the results of a theoretical thermal stress analysis. The theoretical analysis uses only fundamental material and growth parameters, but the "stress-conversion-coefficient" is determined empirically. Ideally, it would be desirable to also calculate the "stress-conversion-coefficient" from fundamental material and growth parameters.

3. What is the origin of the ubiquitious "W" shape for radial EL2 density profiles?

> GaAs possesses a zincblende structure. Under stress, materials with this crystal structure display a two-dimensional stress pattern which resembles a four-leaf clover. If the stress is plotted along a diameter, it will possess a characteristic "W" shape. Since the stress is directly related to the EL2 concentration, then the EL2 profile is also "W" shaped.

54

4.   Can the "W"-shaped EL2 concentration profile be made
constant?

   EL2 diffusing in GaAs possesses a rather high diffusion
   coefficient.   Thus,   whole boule annealing of GaAs can
   be used to reduce the variation in EL2 concentration.

5.   Does   the   compensation between the "W" shaped EL2
concentration profile and the constant carbon concentration
result in variation in electrical parameters?

   As   one   might expect,   the extremes of the EL2
   concentration   curve display the greatest deviation in
   Fermi-level and resistivity.

6. Is the compensation between EL2 and carbon thermally stable?

   The only effect of long term (greater than one hour)
   thermal anneal is to reduce the variations in the EL2
   density profile.   Thus, not only is the compensation
   thermally stable, but the material tends to get better
   as it is annealed.

   Semi-insulating   Gallium Arsenide substrates offer   the

advantages of device isolation, low interconnect capacitance,

simplified processing, and direct ion-implantation for device

fabrication.   Hopefully the results of this project will aid in

improving the quality and homogeneity of existing SI-LEC material

in order to help achieve the tremendous advantages of GaAs

technology.

REFERENCES

1. B. Tuck, "Diffusion and Type Conversion", Semi-Insulating III-V Materials, Kah-nee-ta (D.C. Look and J.S. Blakemore, eds.); Shiva Publishing, Nantwich, pp. 2-18 (1984).

2. D.E. Holmes, R.T. Chen, K.R. Elliott, C.G. Kirkpatrick, and Phil Won Yu, "Compensation Mechanisms in Liquid Encapsulated Czochralski GaAs: Importance of Melt Stoichiometry", IEEE Transactions on Electron Devices, Vol. ED-29, No. 7, pp.1045-1050, July 1982.

3. R.T. Blunt, S. Clark and D.J. Stirland, "Dislocation Density and Sheet Resistance Variation Across Semi-Insulating GaAs Wafers", IEEE Transactions on Electron Devices, Vol. ED-29, No.7, pp. 1039-1044, July 1982.

4. J. Parsey, Y. Naminski, J. Lagowski, and H. Gatos, "Electron Trap-Free Low Dislocation Melt-down of GaAs", Journal of the Electrochemical Society, Volume 128, pg 936-7, (1981).

5. H.M. Hobgood, R.N. Thomas, B.L. Barrett, G.W. Eldridge, M.N. Sopira, and M.C. Driver, Proceedings of Semi-Insulating III-V Materials Conference, Kah-nee-ta, Oregon, Edited by D.C. Look and J.S. Blakemore (Shiva) Nantwich, UK, 1984, pg. 149.

6. C.G. Kirkpatrick, R.T. Chen, D.E. Holmes, and K.R. Elliott, "Growth of Bulk GaAs", published in Gallium Arsenide: Materials, Devices and Circuits, edited by M.J. Howes and D.V. Morgan, John Wiley and Sons, pg 85, (1985).

7. D.E. Holmes, R.T. Chen, K.R. Elliott, C.G. Kirkpatrick, and Phil Won Yu, "Compensation Mechanisms in Liquid Encapsulated Czochralski GaAs: Importance of Melt Stoichiometry", IEEE Transactions on Electron Devices, Vol. ED-29, No. 7, pp.1045-1050, July 1982.

8. R.T. Blunt, S. Clark and D.J. Stirland, "Dislocation Density and Sheet Resistance Variation Across Semi-Insulating GaAs Wafers", IEEE Transactions on Electron Devices, Vol. ED-29, No.7, pp. 1039-1044, July 1982.

9. T.W. Sigmon, "Modeling of Substrate and Implantation Effects on the Threshold Voltage of MESFET Structures Fabricated in Semi-Insulating GaAs", Quarterly Report for Period January 4, 1986 to April 4, 1986, submitted to the United States Air Force, Wright Patterson AFB, Ohio, as part of Contract #F33615-84-C-5072.

10. D.E. Holmes, R.T. Chen, K.R. Elliott, C.G. Kirkpatrick, and Phil Won Yu, "Compensation Mechanisms in Liquid Encapsulated Czochralski GaAs: Importance of Melt Stoichiometry", IEEE Transactions on Electron Devices, Vol. ED-29, No. 7, pp.1045-1050, July 1982.

11. J. Lagowski and H. Gatos, "Nonstoichiometric Defects in GaAs and the EL2 Bandwagon", 13th International Conference on Defects in Semiconductors, Coronado CA, August 1984.

12. G. Martin, A. Mitonneau and A. Mircea, "Electron Traps in Bulk and Epitaxial GaAs Crystals", Electronics Letters, March 31, 1977, Volume 13, Number 7, pg 191-192.

13. G. Martin, J. Farges, G. Jacob and J. Hallis, "Compensation Mechanisms in GaAs", Journal of Applied Physics, 51(5), May 1980, pg 2840.

14. D.E. Holmes, and R.T. Chen, "Contour Maps of EL2 Deep Level in Liquid Encapsulated Czochralski GaAs", Journal Applied Physics, 55(10), 15-May-1984, pg. 3588-3594.

15. G.M. Martin, G. Jacob, G. Poibaud, A. Goltzene, and C. Schwab, "Identification and Analysis of Near-infrared Absorption Bands in Undoped and Cr-doped Semi-insulating GaAs Crystals", Defects and Radiation Effects in Semiconductors, 1980 (Oiso), Institute of Physics Conferences, Serial 59, Bristol and London, Institute of Physics (1981).

16. D.E. Holmes, R.T. Chen and J. Yang, "EL2 Distributions in Doped and Undoped Liquid Encapsulated Czochralski GaAs", Applied Physics Letters, 42(5), 1-March-1983, pg. 419-421.

17. M.R. Brozel, I. Grant, R.M. Ware, D.J. Stirland, and M.S. Skolnik, "Direct Observation of Fine Structure in the Concentration of the Deep Donor [EL2] and its correlation with Dislocations in Undoped, Semi-Insulating GaAs", J. Applied Physics 56(4), pp. 1109-1118, 15 August 1984.

18. A.S. Jordan, R. Caruso, and A.R. von Neida, "A Thermoelastic Analysis of Dislocation Density in Pulled GaAs Crystals", Bell System Technical Journal, Vol. 59, pg. 593, 1980.

19. K. Kitahara, K. Nakai, and S. Shibatomi, "One-dimensional Photoluminescence Distribution in Semi-Insulating GaAs Grown by CZ and HB method", Journal of the Electrochemical Society, Volume 129, April 1982, pg 880-883.

20. R.T. Blunt, S. Clark and D.J. Stirland, "Dislocation Density and Sheet Resistance Variation Across Semi-Insulating GaAs Wafers", IEEE Transactions on Electron Devices, Vol. ED-29, No.7, pp. 1039-1044, July 1982.

21. Skolnick, M.R. Brozel, I. Grant, D.J. Stirland, and R.M. Ware, "Inhomogenity of EL2 in GaAs observed by Direct Infrared Imaging", Electronic Materials Conference, Burlington, VT, Abstracts, pp. 75-76 (1983)

22. G.M. Martin, G. Jacob, G. Poibaud, A. Goltzene, and C. Schwab, "Identification and Analysis of Near-infrared Absorption Bands in Undoped and Cr-doped Semi-insulating GaAs Crystals", Defects and Radiation Effects in Semiconductors, 1980 (Oiso), Institute of Physics Conferences, Serial 59, Bristol and London, Institute of Physics (1981).

23. E.R. Weber, H. Ennen, U. Kaufmann, J. Windshief, J. Schneider, and T. Wasinki, "Indentification of As/Ga Antisites in Plastically Deformed GaAs, Journal of Applied Physics, 53(9), September 1982, pg.6140-6143.

24. J. Parsey, Y. Naminski, J. Lagowski, and H. Gatos, "Electron Trap-Free Low Dislocation Melt-down of GaAs", Journal of the Electrochemical Society, Volume 128, pg 936-7, (1981).

25. R.T. Chen and D.E. Holmes, "Dislocation Studies in 3-inch diameter Liquid-Encapsulated-GaAs", Journal of Crystal Growth, Volume 61, 1983, pg. 111-124.

26. A.S. Jordan, R. Caruso, and A.R. von Neida, "A Thermoelastic Analysis of Dislocation Density in Pulled GaAs Crystals", Bell System Technical Journal, Vol. 59, pg. 593, 1980.

27. M.R. Brozel, I. Grant, R.M. Ware, D.J. Stirland, and M.S. Skolnik, "Direct Observation of Fine Structure in the Concentration of the Deep Donor [EL2] and its correlation with Dislocations in Undoped, Semi-Insulating GaAs", J. Applied Physics 56(4), pp. 1109-1118, 15 August 1984.

28. D.E. Holmes, and R.T. Chen, "Contour Maps of EL2 Deep Level in Liquid Encapsulated Czochralski GaAs", Journal Applied Physics, 55(10), 15-May-1984, pg. 3588-3594.

29. D.E. Holmes, H. Kuwamkoto, C.G. Kirkpatrick, and R.T. Chen, "Effect of Thermal History on Properties of LEC GaAs", Publication of Rockwell International Corporation, Microelectronics Research and Development Center, 1984, pg. 204-213.

30. D.E. Holmes, and R.T. Chen, "Contour Maps of EL2 Deep Level in Liquid Encapsulated Czochralski GaAs", Journal Applied Physics, 55(10), 15-May-1984, pg. 3588-3594.

END

5 - 87

DTIC